Polymer Vol. 38 No. 12, pp. 2957–2967, 1997

0032-3861/97/$17.00 + 0.00

PII: S0032-3861(96)00852-X

Metastable polymer blends by precipitation with a compressed fluid antisolvent

Simon Mawson, Sanjay Kanakia and Keith P. Johnston*
Department of Chemical Engineering, University of Texas, Austin, TX 78712, USA
(Received 21 December 1995; revised 31 August 1996)

Metastable polymer blends of polycarbonate (PC) and poly(styrene-*co*-acrylonitrile) (SAN) are formed by spraying polymer solutions into liquid and supercritical fluid CO_2. Because of the rapid mass transfer between the CO_2-phase and the solution phase, the blends are trapped in a metastable state before they can phase separate. A transition from a metastable blend with a single glass transition temperature, T_g in the form of particles, to a phase-separated 100 μm fibre is observed with an increase in polymer concentration from 3.0 to 9.0 wt%. This transition is related to the calculated concentration for the dilute to semi-dilute transition, C^*, of PC/SAN in THF and the characteristic times for polymer–polymer and polymer–solvent phase separation. PC and SAN do not form a blend at 35°C because of plasticization by CO_2. They also do not form a metastable blend when 1.0 mm droplets are precipitated into a liquid antisolvent, heptane.

(Keywords: metastable polymer blend; compressed fluid; phase separation)

INTRODUCTION

Most polymer pairs do not form miscible blends since the entropic driving force is small. Poor interfacial adhesion severely limits the mechanical integrity of such immiscible polymer blends. One method to form a blend is to compatiblize the components with a block copolymer. For example, block copolymers composed of poly(glycolic acid) and poly(L-lactic acid) may be tailored to blend these homopolymers. These blends are of interest for controlling the release rate in drug delivery applications[1]. Our approach is to precipitate two polymers from solution rapidly with an antisolvent to trap a miscible blend in a metastable state, without the need for a surfactant compatibilizer.

Metastable polymer blends may be formed by rapidly flashing a liquid solution, or a supercritical solution. Rapid flash devolatilization, called 'compositional quenching', was used to produce a variety of metastable rubber in polymer microdispersions from homogeneous liquid solutions[2]. Because the flash temperatures were between 185 and 290°C, it was necessary for the polymer matrix to have a high viscosity after the flash to prevent polymer–polymer phase separation. In addition, poly(ethyl methacrylate) (PEMA) and poly(methyl methacrylate) (PMMA) have been trapped in a metastable blend by rapid expansion from a supercritical solution (RESS)[3]. In RESS, phase separation occurs due to a mechanical perturbation created when the supercritical solution expands across a fine throttling device, such as a capillary or orifice nozzle[3–9]. Unlike the case for compositional quenching, the blends formed by RESS were recovered as a powder at room temperature.

In supercritical fluid technology, CO_2 is the preferred solvent, because it has a low critical temperature, T_c = 31°C, and is non-flammable, relatively non-toxic, and environmentally benign. The only high molecular weight polymers that are significantly soluble in CO_2 below 50°C are poly(fluoroacrylates) and poly(dimethyl siloxanes)[9–11]. Recently, a semicrystalline fluoroacrylate polymer, poly(1,1,2,2-tetrahydroperfluorodecylacrylate) (poly(TA-N)) was expanded from CO_2 to produce a variety of submicron particles and fibrils. The morphology was related to the location of phase separation within the expansion nozzle to understand better the mechanism in RESS[9]. In all other RESS studies, more polarizable SCF solvents, including low molecular weight alkanes, alkenes and chlorofluorocarbons were utilized at temperatures well above 100°C[3–8,12,13].

The solubility limitations in RESS may be overcome with a newer process, precipitation with a compressed fluid antisolvent (PCA). Since PCA uses common organic solvents, a variety of polymers can be dissolved at ambient temperature. Once dissolved the homogeneous polymer solution is sprayed through an atomization device, i.e. either a capillary nozzle[14], orifice[15], or a sonicator[16], into the co-currently flowing CO_2 antisolvent. The rapid two-way mass transfer of the CO_2 in and organic out of the polymer solution facilitates the rapid phase separation of the polymeric solute. Because CO_2 is such a small molecule, and has such a low viscosity, two-way diffusion is much faster than in the case of conventional liquid antisolvents. The rapid nucleation leads to materials with small features and high surface areas, which are rarely produced with conventional liquid antisolvents. PCA has been used to produce 100 nm–4.0 μm microspheres and microparticles of a variety of polymers including amorphous polystyrene[14,17] and semicrystalline L-PLA[16,18].

Our objects are: (1) to form metastable polymer blends for the first time by PCA, and (2) to characterize the kinetics of the PCA process in terms of the degree of

*To whom correspondence should be addressed

phase separation of the polymers in the blend. Carefully controlled experiments have been performed to understand the jet breakup (as a function of the solution viscosity), the mass transfer pathway through the phase diagram, the characteristic time for polymer/solvent phase separation *versus* diffusion of the two polymers into separate phases, and the plasticization of the polymer by CO_2 (and residual solvent). The glass transition behaviour of the products is characterized by d.s.c., while the morphology is determined by SEM. To calibrate the d.s.c. results, samples of the pure component homopolymers were prepared by PCA. To study the effect of plasticization of the polymers by CO_2, the temperature was varied from 0 to 35°C. The polymer weight fraction in the solvent (for a 50/50 polymer mixture) was varied from 0.5 to 9.0 wt% to understand how jet break-up and mass transfer influence the blend formation. Finally, experiments were performed to compare heptane as an antisolvent to CO_2 to contrast the PCA technique with conventional antisolvent precipitation. Heptane was selected as an antisolvent as it is not expected to form any specific interactions with either polycarbonate (PC) or poly(styrene-acrylonitrile) (SAN), which may otherwise hinder phase separation[19].

CO_2 is a potent plasticizer for amorphous polymers[20–23]. Plasticization can limit the ability to trap a glassy blend in a metastable state. To avoid this, the experimental temperature must be in a region where the polymers are glassy for a given CO_2 pressure. Otherwise, even if a metastable blend is formed in the jet it will not be quenched to a glassy state, which is required to prevent phase separation. Given these considerations, we have chosen to study the polycarbonate ($M_W = 64\,000$)–poly(styrene-*co*-acrylonitrile) ($M_W = 152\,000$, 25 wt% acrylonitrile) mixture in tetrahydrofuran. This system presents a significant challenge as these polymers are highly immiscible. A related system, polycarbonate-polystyrene, is also difficult to blend[24]. However, we were unable to use this system because of the low mutual solubility of both polycarbonate and polystyrene in THF.

EXPERIMENTAL

Materials

The polycarbonate (PC) was purchased from Scientific Polymer Products (SPP) and had a M_W of 64 000 and a T_g of 148°C. The poly(styrene-*co*-acrylonitrile) (SAN), containing 25 wt% acrylonitrile (Tyril 1000, Dow Chemical Co.) had a M_W of 152 000 and T_g of 110°C. Additional properties are shown in *Table 1*. Tetrahydrofuran (THF) (reagent grade) was used as the common solvent for both PC and SAN. Heptane (reagent grade) was selected for the conventional antisolvent experiments. Instrument grade CO_2 was used as received.

Oligomer impurities in SAN can cause PC/SAN systems to become partially miscible[25]. Therefore, SAN was extracted according to the method suggested by Callaghan *et al.*[25] SAN was dissolved in methyl ethyl ketone (MEK) (Mallinkrodt) and precipitated into an excess of methanol (EM Science) three times. D.s.c. analysis indicated that the T_g of SAN increased between 4 and 6°C after extracting the oligomers.

Apparatus and procedure

In previous experiments[14–16,26], the morphologies of products made by PCA were analysed by scanning electron microscopy (SEM). Because SEM requires minute amounts of sample, spray times have been typically $\leq$ 1 min. However, for d.s.c. analysis, 5–10 mg of sample are required; therefore, the PCA apparatus was modified to collect larger polymer samples, typically 0.5–1.0 g.

Figure 1 shows the experimental apparatus for precipitating the PC/SAN mixtures. A high pressure vessel of 300 ml internal volume equipped with a magnetically coupled agitator (Parr) was used as a precipitator. A 1.27 cm i.d. sapphire tube with an internal volume of 13 ml was also used to observe the precipitation of the PC–SAN/THF solutions visually. Details of this vessel and the sampling technique used to collect the polymer precipitate for SEM analysis have been described elsewhere[17,26].

The polymer solution was sprayed through either 50 or 100 μm i.d. fused silica capillary tubing (Polymicro Technology) with various length/diameter (l/d) ratios from 10^3 to 10^2. Each capillary was inspected with a microscope to ensure a smooth tip. For dilute solutions,

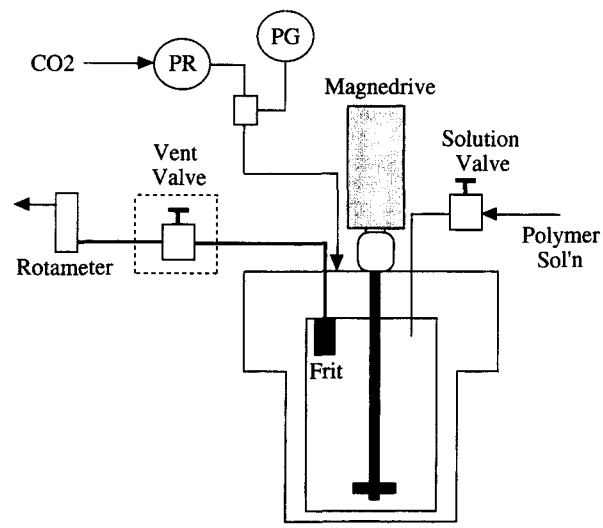

Figure 1 Stirred apparatus for preparing large samples by precipitation with a compressed fluid antisolvent (PCA). PR, pressure regulator; PG, pressure gauge

Table 1 Physical properties of polymers in CO_2 at 25°C and 67 bar

Polymer	Designation	M_W	S (CO_2)[a] (g/100 g polymer)	T_g (°C)	T_g[b] (°C)
Poly(styrene-*co*-acrylonitrile)	SAN	152 000	16.5	110, 115[c]	NA
Polycarbonate	PC	64 000	14.0	148	NA
Polystyrene	PS	280 000	12.5	100	31

[a] Sorption data from Berens *et al.*[28]
[b] T_g in the presence of CO_2, from Condo *et al.*[22]
[c] After oligomer extraction

a Milton-Roy high pressure reciprocating pump was used in conjunction with a back pressure regulator (Tescom, model 26-1021) to inject the polymer solution through the capillary into the flowing CO_2. Because the pumping assembly was prone to plugging for concentrated polymer solutions, solutions above 3.0 wt% were injected with a cylindrical 0.688″ i.d. × 8″ vessel (Autoclave) fitted with a piston containing two 90 durometer buna-n O-rings. CO_2 was used as the pressurizing fluid for the piston. Solution flowrates were determined by recording the amount of time required to collect a volume of solution sprayed into ambient conditions. For a constant pressure drop, flowrates were assumed to be constant.

A 0.5 μm filter prevented loss of the precipitate from the precipitation vessel. The filter assembly was comprised of an in-line sintered filter element (Swagelok 'F' series) which was welded onto a 1/4″ i.d. NPT fitting. The frit assembly was threaded into the CO_2 effluent port located in the bottom of the precipitation vessel. The effluent vent value (Whitey, SS-21RS4) was heated in a water bath to >50°C to prevent the expanding CO_2 from freezing. The CO_2 flowrate was measured with a rotameter (Omega, model #FLT-40ST). Upon completion of the solution spray, approximately three residence volumes of liquid CO_2 (900 ml) were pumped through the precipitator to remove residual organic solvent. Agitation was maintained throughout the spraying and drying stages. However, agitation was always discontinued during depressurization. After drying, the precipitation vessel was isolated and allowed to depressurize for 30–45 min.

For the experiments involving liquid antisolvents, the polymer solution was atomized into the organic antisolvent with the pumping apparatus described above. The tip of the atomizer was always maintained below the surface of the antisolvent which was stirred. In a second type of experiment, a 100 ml burette was used to produce large droplets of the polymer solution which fell into the antisolvent. The tip of the burette was placed above the liquid antisolvent. Droplet sizes were estimated visually.

Characterization

The T_g behaviour of each product was determined with a Perkin Elmer DSC-7 differential scanning calorimeter. D.s.c. samples ranged in weight from 5 to 15 mg and were heated at 20°C min^{-1} from 25 to 200°C. For PC/SAN samples heated above 275°C, CO_2 did not induce crystallization of the PC[27]. The polymer morphology was analysed on a Jeol JSM-35C scanning electron microscope. Samples were sputter coated with gold–palladium to a thickness of approximately 200 Å.

RESULTS AND DISCUSSION

Pure component PC and SAN behaviour

In order to characterize the sub-T_g enthalpy relaxation or prior history of the blend homopolymers, solutions of 3.0 wt% PC and SAN, each in THF solution, were sprayed into CO_2 at 23°C ($\rho = 0.85$ g cm^{-3}). The precipitated PC and SAN samples were analysed by d.s.c. at three conditions: (1) no preheat, to discern the effects of PCA on the sub-T_g peak, (2) a sub-T_g preheat to $T < T_g$ of the homopolymer, to partially anneal the polymer, and (3) a 200°C preheat. Because the 200°C preheat removes all PCA prior history effects, it may be used to determine the actual PC and SAN T_g. With the metastable PC/SAN blends, the prior history cannot be removed by thermal annealing at $T > T_g$ of the PC, as the blend would relax into its phase separated, equilibrium state. As suggested by a reviewer, the T_g and sub-T_g endotherm could be separated by using a modulated d.s.c. A summary of the conditions studied and the T_g behaviour, with an uncertainty within ±3°C is presented in *Table 2*.

Figure 2 shows the d.s.c. thermal curves of SAN (unextracted) precipitated by PCA. A large endothermic sub-T_g peak is observed for the SAN after PCA when no preheat is used. Preheating the SAN to 100°C has little effect upon the location or magnitude of the sub-T_g peak. Sub-T_g peaks primarily reflect the effects of free volume arrangements. Berens *et al.*[28] have performed a detailed investigation into the effect of different pretreatments upon the prior history of glassy poly(vinyl chloride). Rapid thermal quenching into liquid nitrogen or high pressure solvent conditioning were shown to produce sub-T_g peaks. PCA involves rapid quenching, along with conditioning by both CO_2 and organic solvent. All of these effects can contribute to the sub-T_g peak. When the SAN sample is annealed at 200°C, well above the pure SAN T_g, the PCA history effects are removed. Comparison of the SAN T_g both before and after removal of the prior history reveals that the occurrence of the sub-T_g peak results in a substantial shift in the location of the apparent T_g. Throughout this study, the apparent T_g is designated as the onset of the step-change in the heat flow which is indicated by dashed lines and arrows. Based upon the 200°C preheat, the actual T_g for SAN after PCA is determined to be 110°C. For lower preheat temperatures, an apparent T_g due to prior history effects occurs between 120 and 126°C.

Figure 3 shows the d.s.c. thermal curves of pure PC precipitated by PCA. The formation of a large PC sub-T_g peak is not observed without preheat. By preheating the sample to 135°C, a small sub-T_g endotherm is produced. The small PC sub-T_g endotherm suggests that the PC contains less trapped free volume than SAN. Consequently, the difference between the location of the actual (200°C preheat) and apparent (no preheat) T_g is smaller for PC than SAN. The actual T_g for PC is 148°C after annealing at 200°C, whereas, the apparent PC T_g is between 152 and 156°C with no preheat and preheat to 135°C.

Effect of blend composition

The d.s.c. thermal curves of 3.0 wt% PC/SAN (50/50) solutions sprayed at 1.0 ml min^{-1} into CO_2 at 23°C are shown in *Figure 4*. The blend T_g is approximately 136°C by the T_g onset method for no preheat. A slight sub-T_g endotherm is apparent. However, the magnitude of the sub-T_g endotherm is significantly smaller than that observed for pure SAN. An annealing technique was used to characterize the miscibility of the PC/SAN blends[29]. The PC/SAN blend was annealed for 12 h at 90°C. The 90°C annealing temperature is closer to the T_g of SAN than either the blend intermediate T_g or the PC T_g. For all annealing longer than 2 h, a large sub-T_g peak formed below the intermediate blend T_g. If the blend had phase separated a distinct SAN enthalpy relaxation peak would have formed below the SAN T_g.

The metastable blends were preheated to higher

Table 2 Summary of T_g behaviour of PC/SAN blends precipitated by PCA and the conventional antisolvent process

Conc. (wt%)	Comp. (PC/SAN)	T (CO_2) (°C)	ρ (CO_2) (g cm^{-3})	Apparent T_g (±3°C-d.s.c.)	Macrostructure
0.5	50/50	23	0.85	134	fine powder
3.0	0/100	0	0.96	110[a], 115[a,b]	fine powder
	30/70	0	0.96	128, 128[b]	fine powder
	50/50	0	0.96	136, 135[b]	fine powder
	50/50	23	0.85	137	fine powder
	50/50	35	0.79	112, 138	fluffy powder
	70/30	0	0.96	141, 140[b]	fine powder
	100/0	0	0.96	148[a]	fine powder
	50/50	0	0.96	134[c]	brittle powder
	50/50	0	0.96	111, 146[d]	brittle powder
6.0	50/50	23	0.85	118, 138	fibrous powder
9.0	50/50	23	0.85	114, 142	continuous fiber

[a] Annealed at 200°C to remove prior history
[b] Extracted SAN
[c] Atomized into heptane
[d] Titrated into heptane

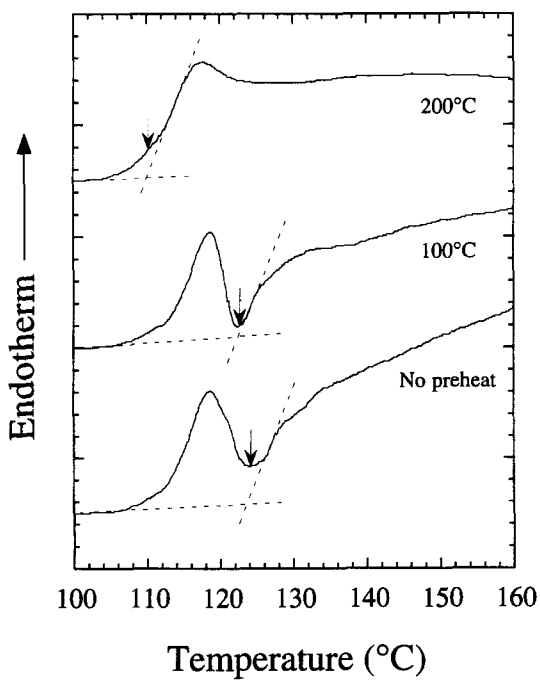

Figure 2 D.s.c. thermal curves of SAN formed by spraying a 3.0 wt% SAN in THF solution at 1.0 ml min^{-1} into CO_2 at 23°C and 107 bar ($\rho = 0.85$ g cm^{-3})

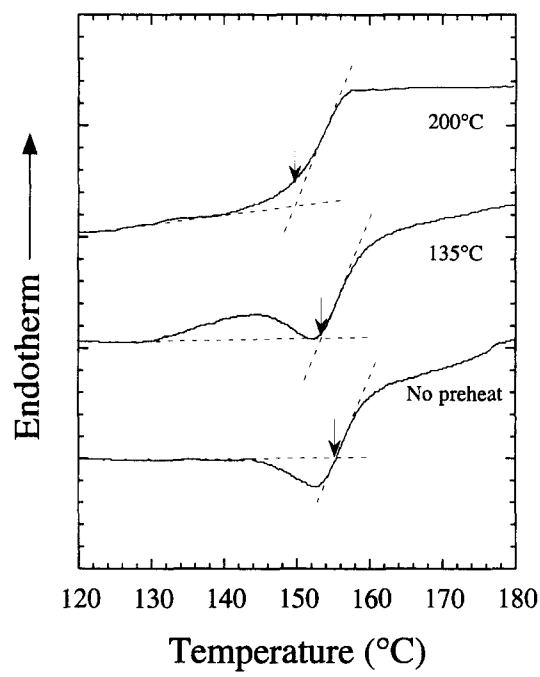

Figure 3 D.s.c. thermal curves of PC formed by spraying a 3.0 wt% PC in THF solution at 1.0 ml min^{-1} into CO_2 at 23°C and 107 bar ($\rho = 0.85$ g cm^{-3})

temperatures above the T_g of both the blend and PC to study their stabilities. When the 3.0 wt% PC/SAN blend was preheated to 110 or 120°C, the location of the T_g remained constant as shown in *Figure 4*, although the magnitude of the sub-T_g endotherm increased. The increasing size of the sub-T_g endotherm with increasing temperature from no preheat to 120°C preheat arises from both SAN and PC enthalpy relaxation, consistent with *Figures 2* and *3*.

Above 120°C, a different relaxation mechanism occurs. At 130°C, the blend begins to phase separate into two discernible T_gs. The appearance of a distinct SAN phase is confirmed after a 130°C preheat, yet no PC T_g is observed. After the 200°C preheat, both SAN and PC T_g peaks are observed indicating that the PC/SAN blend relaxes towards the equilibrium phase separated state. Because the pure component SAN T_g is 110°C, the 120, 130 and 140°C preheats transform the glassy SAN into the rubbery state. However, at these conditions the PC remains as a rigid glass since its pure component T_g is 148°C. At the 110 and 120°C preheat, slight relaxation of the SAN occurs, but the rigid PC matrix prevents significant SAN diffusion into a discernible new phase. At 130°C, the SAN has sufficient thermal energy to relax and also diffuse away from the rigid PC matrix. Because the PC remains in the glassy state up to 150°C, the 140°C preheat does not allow the PC to relax into a PC-rich phase. Instead, the diffusion of the PC is dependent upon the highly mobile SAN. At the 200°C preheat, the PC also relaxes to the equilibrium state as evidenced by the appearance of two pure component d.s.c. peaks.

The composition dependence of the T_g behaviour for a 3.0 wt% PC/SAN blend sprayed into CO_2 at 0°C is shown by the d.s.c. thermal curves in *Figure 5*. The pure component PC (100/0) and SAN (0/100) scans were obtained after 200°C preheat. The d.s.c. scans shown for the 30/70, 50/50 and 70/30 PC/SAN blends were obtained by directly heating the PCA precipitate to 200°C without preheat. An increase in blend T_g with increasing PC composition for the PC/SAN blends using both as received (solid lines) and extracted (dashed lines) SAN is observed as expected. Although *Table 2* shows that the extracted SAN T_g (0/100) is ~5°C above that of the as received SAN T_g, the extraction of SAN oligomers has an apparently very small effect upon the location of the blend T_g. The sub-T_g peak observed for the 70/30 as received PC/SAN blend arises from annealing in the d.s.c. at 80°C for 5 h.

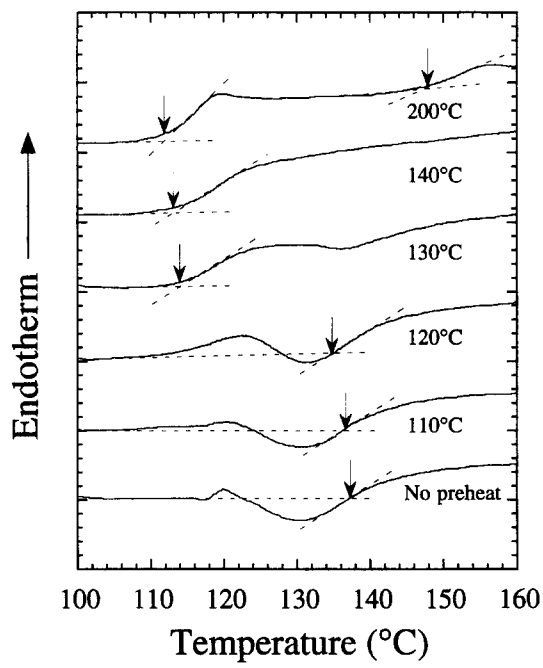

Figure 4 D.s.c. thermal curves of a preheated PC/SAN blend formed by spraying a 3.0 wt% (50/50) PC/SAN in THF solution at 1.0 ml min^{-1} into CO_2 at 23°C and 107 bar

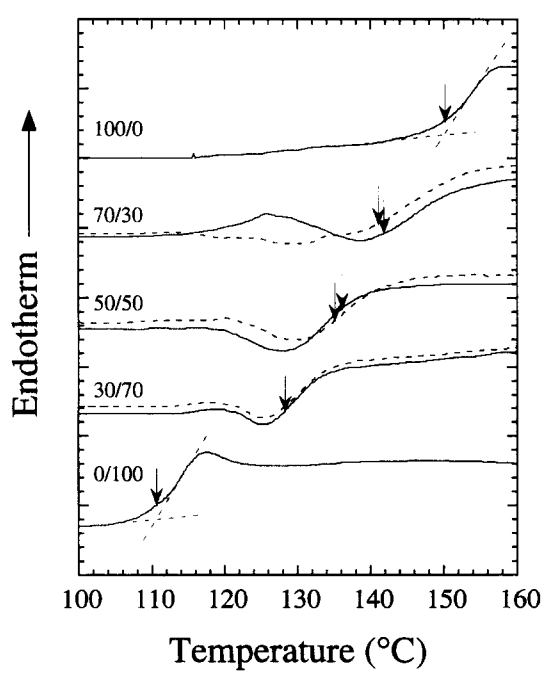

Figure 5 D.s.c. thermal curves of PC/SAN blends formed by spraying various composition 3.0 wt% PC/SAN in THF solutions at 1.0 ml min^{-1} into CO_2 at 0°C. (—) As received SAN; (- - -) extracted SAN

The T_g behaviour for the PC/SAN blends is shown more clearly in *Figure 6* where the T_g is plotted against the weight fraction of PC in the blend. *Table 2* also shows the T_g prediction of the simple Fox equation which is given by $1/T_g = w_1/T_{g1} + w_2/T_{g2}$, where w_1 and w_2 are the weight fractions of the components[30]. As shown in *Figure 6*, the apparent T_g for each of the blend compositions falls above the Fox prediction (—) when the pure component T_g values for SAN and PC of 110 and 148°C, respectively, are used to determine the blend T_g. When the value of 115°C for the extracted SAN is substituted into the Fox equation, the blend T_g is also underpredicted (- - -). This shift in the blend T_g to ~2–7°C above the Fox prediction arises from excess free volume trapped in the blend by the rapid PCA quench. The shifts in the actual pure component SAN and PC T_g values due to rapid quenching were illustrated in *Figures 2* and *3*. If the un-annealed SAN and PC T_g values of 123 and 155°C are used in the Fox equation, *Figure 6* shows that the T_g behaviour was only slightly overpredicted (- - -).

Effect of CO_2 *plasticization*

The effect of plasticization by CO_2 was investigated by spraying a 3.0 wt% (50/50) PC/SAN solution into CO_2 at 0, 23 and 35°C as shown in *Figure 7*. When the CO_2 temperature was maintained at 0°C ($\rho_{CO_2} = 0.96\,g\,cm^{-3}$) and 23°C ($\rho_{CO_2} = 0.85\,g\,cm^{-3}$), a single phase metastable blend was formed. At 35°C ($\rho_{CO_2} = 0.80\,g\,cm^{-3}$), two individual glass transitions are observed. As shown in *Table 2*, the PC/SAN blend at 35°C was fluffy, whereas, at 0 and 23°C a fine powder was observed. Similar trends in the morphology have been observed when PS microspheres were precipitated into CO_2 at temperatures above and below the depressed T_g of PS[14].

Although the T_g behaviour of a PC/SAN blend in CO_2 is unknown, it may be approximated from the solubility of CO_2. CO_2 solubility data in the constituent homopolymers have been obtained at liquid CO_2 conditions[28], for PC, SAN and PS at 25°C and 67 bar, as shown in *Table 1*. The T_g depression reported for PS was determined *in situ* by using creep compliance experiments[22]. The CO_2 solubility in PS results in a T_g depression to ~31°C, for $P > 60$ bar.

As shown in *Table 1*, the solubility of CO_2 in PC (14.0 wt%) and SAN (16.5 wt%) compares favourably to the level found in PS. The increase in CO_2 solubility in PS from 12.5 to 16.5 wt% with the addition of 25 wt% poly(AN), may be due to weak nitrile–CO_2 specific interactions[28]. The strength of donor–acceptor interactions between CO_2 and Lewis bases been found to be weak compared to those for other Lewis acids such as trichloromethane[31]. Also, poly(AN) is a semicrystalline polymer and has been found to show none of the signs of plasticization when precipitated into CO_2 at temperatures as high as 40°C[26]. Based on T_g data for PS plasticized by CO_2 and the sorption of CO_2 in AN, it is quite reasonable that the SAN copolymer (75 wt% styrene) was plasticized at 35°C and not at 23°C, as suggested by the d.s.c. data. For PC, the CO_2 sorption (14.0 wt%) is

only slightly higher than in PS. Although a slightly higher T_g depression has been observed in PC than PS, the high pure component T_g of 150°C is expected to prevent depression of T_g for PC below 30°C[32]. The organic solvent in the PCA precipitator could also contribute to the depression in the T_g before the particles were fully dried by CO_2. However, the lack of phase separation at 23°C suggests the blend was not plasticized.

Effect of solution concentration

The d.s.c. thermal curves in *Figure 8* show the results of increasing the concentration of the PC/SAN (50/50) in THF solution from 0.5 to 9.0 wt% at 23°C. A homogeneous blend was produced when 0.5 and 3.0 wt% PC/SAN solutions were precipitated. *Table 2* shows that the macrostructure of these PC/SAN precipitates was a powder. The microstructures of the 0.5 and 3.0 wt% powders are depicted in the SEM micrographs shown in *Figure 9*. The 0.5 wt% PC/SAN solution produced polymer microparticles with an average particle size $<1.0\,\mu m$ (*Figure 9A*). *Figure 9B* shows that the average particle size of the 3.0 wt% PC/SAN precipitate is $\geq 10.0\,\mu m$. A higher magnification revealed no discernible primary particles. During the spray, the 0.5 wt% PC/SAN solution was observed to atomize into a uniform, fine mist. Atomization is observed for the 3.0 wt% PC/SAN solution, although, a slightly fibrous precipitate is also observed. For a PC/SAN concentration of 6.0 wt%, the d.s.c. scan reveals a transition from a single-T_g blend to a partially phase separated mixture. The morphology consists of $100\,\mu m$ broken, short fibres. For a 9.0 wt% solution, the d.s.c. scan reveals nearly complete polymer phase separation, as two T_gs are observed at approximately 110 and 150°C. A long continuous $100\,\mu m$ fibre was formed at this concentration.

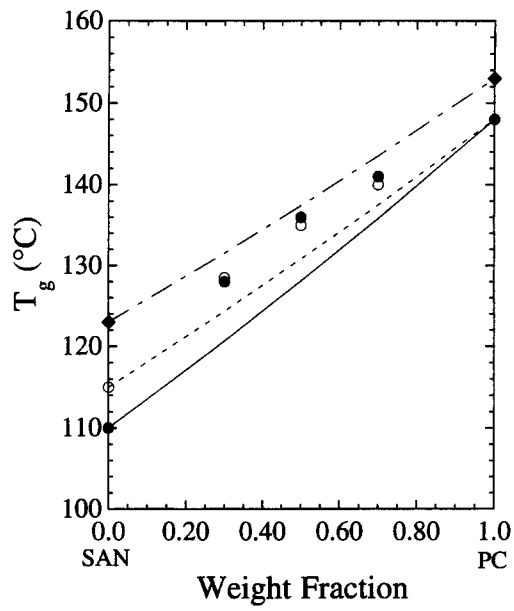

Figure 6 T_g behaviour for various composition 3.0 wt% PC/SAN blends sprayed at 1.0 ml min^{-1} into CO_2 at 0°C ($\rho = 0.96\,g\,cm^{-3}$) as determined by d.s.c. at 20°C min^{-1} using the onset method. (●) As received SAN, (○) extracted SAN. (—) As received SAN T_g, (- - -) extracted SAN T_g, (- – -) T_g without annealing

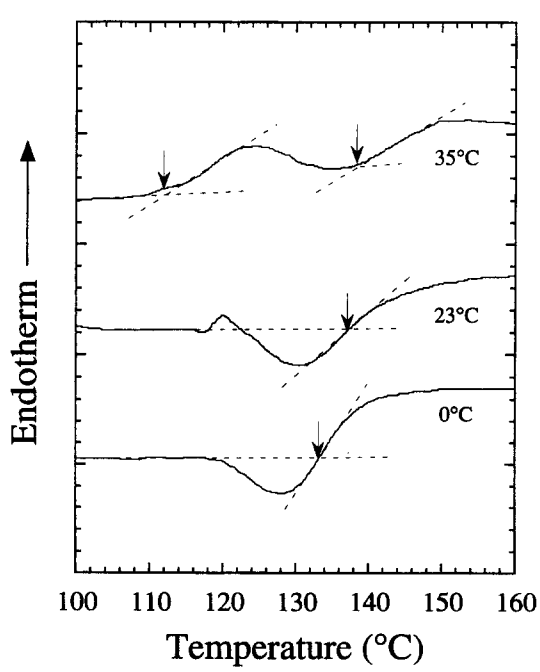

Figure 7 D.s.c. thermal curves of a 3.0 wt% (50/50) PC/SAN sprayed at 1.0 ml min^{-1} into CO_2 at 0, 23 and 35°C

We now propose a mechanism for blend formation. It begins with the viscosity of the PC/SAN solution, which is directly related to the PC/SAN concentration in THF. As the solute concentration increases, the increase in solution viscosity changes the jet hydrodynamics from atomization to the formation of a single fibre. The breakup mechanism of the jet directly affects the size of the PC/SAN domains to be quenched by the CO_2 antisolvent. In addition, the domain sizes produced by the jet affect the time required for polymer–solvent phase separation. Because the polymers are immiscible, it is crucial that the time for polymer–solvent phase separation is faster than the time for polymer–polymer phase separation. Otherwise the constituent polymers will phase separate. Therefore, the degree of polymer–polymer phase separation provides an indirect measure of the characteristic time for polymer–solvent phase separation.

It is useful to examine the mechanism for jet breakup in greater detail. For a solution of given composition, the PCA jet breakup mechanism is described by the dimensionless Weber number (N_{We}), Ohnesorge number (N_{Oh}) and Reynolds number (N_{Re})[14,26]. The N_{We} is the ratio of the inertial forces to surface tension forces and is given by $N_{We} = \rho_A v^2 D/\gamma$ where ρ_A is the antisolvent density, v is the velocity of the jet relative to that of the CO_2, D is the jet diameter, and γ is the interfacial tension. The Ohnesorge number N_{Oh} or ratio of viscous to interfacial forces is defined by $N_{Oh} = N_{We}^{1/2}/N_{Re} = \eta/(\rho D\gamma)^{1/2}$, where η is the solution viscosity[33,34]. At high values of N_{Oh} and N_{Re}, the jet breaks up by atomization and has been shown to favour the formation of 0.1–4.0 μm particles and spheres[14–16,18]. At low values of N_{Oh} and N_{Re}, jet breakup is greatly reduced favouring the formation of hollow and porous solid fibres[26,35].

Previous studies of PCA by Dixon *et al.*[14,35] and Luna-Bàrcenas *et al.*[26] have measured the solution viscosity to evaluate the effect of N_{Oh}. To determine the solution viscosity, the non-Newtonian viscosity $\eta(\gamma)$ at the wall of the capillary is determined as a function of shear rate, γ, and concentration for PC/SAN in THF solutions as shown in *Figure 10*. A decrease in the solution viscosity is observed with an increase in shear rate for each PC/SAN

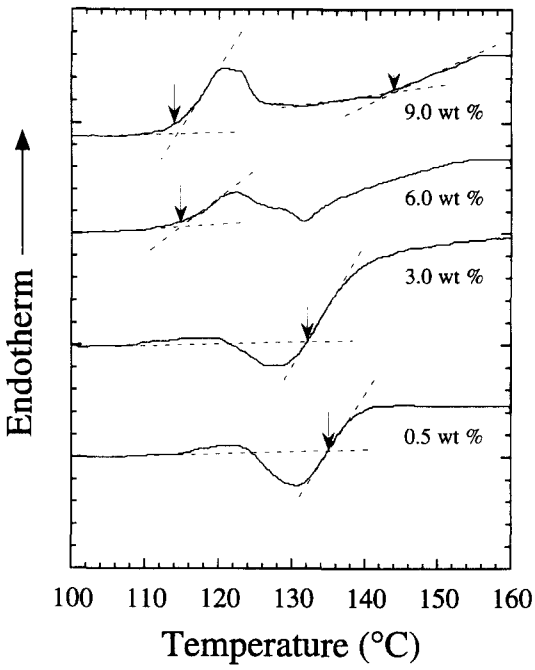

Figure 8 D.s.c. thermal curves of 50/50 PC/SAN blends formed by spraying various concentration PC/SAN in THF solutions at 1.0 ml min^{-1} into CO_2 at 23°C and 107 bar

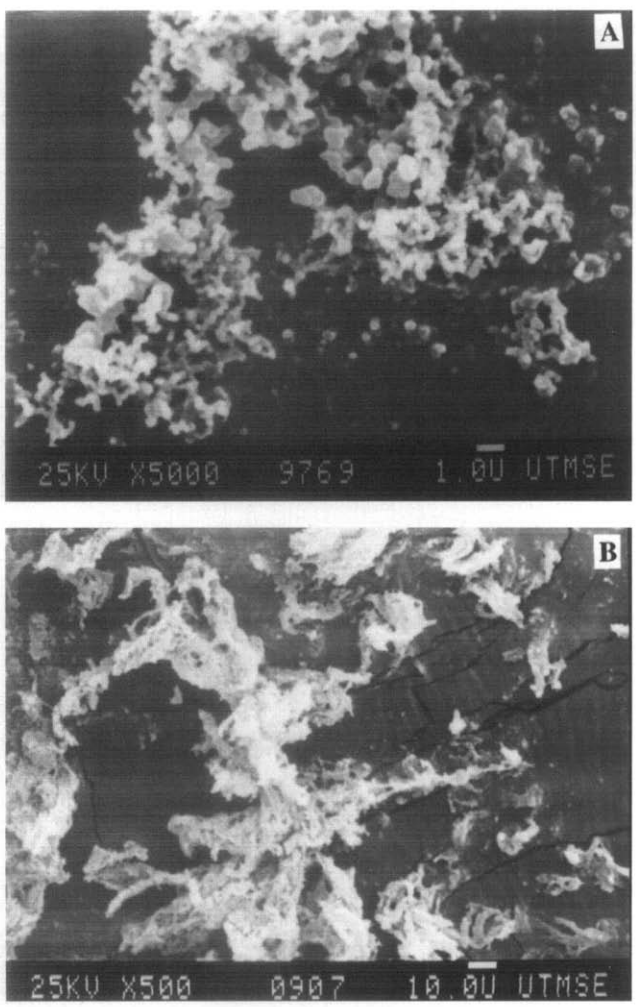

Figure 9 SEM micrographs showing the morphology of (A) 0.5, (B) 3.0 wt% PC/SAN blends sprayed at 1.0 ml min^{-1} into CO_2 at 23°C and 107 bar

concentration. At a constant shear rate of 10^6 s^{-1}, the solution viscosity increases by a factor of 3 as the polymer concentration is increased from 0.5 to 3.0 wt%. As shown in *Figure 9*, and in the above visual observations, this change in the solution viscosity has a dramatic effect upon the jet breakup and the microstructure of the PC/SAN morphology. The larger 10 μm particles produced at 3.0 wt% suggest that partial chain entanglement has occurred. The visual observation of a slightly fibrous precipitate at 3.0 wt%, confirmed that a shift toward a polymer continuous morphology has started.

We now estimate the solution concentration range for the particle to fibre transition as a function of the dilute to semi-dilute transition concentration, C^*[26]. At C^*, polymer chains no longer exist in discrete domains, but become entangled. The location of C^* is illustrated on the ternary phase diagram shown in *Figure 11*. The phase diagram is bounded by three regions; the one-phase region located between the polymer/solvent axis and the binodal line, the metastable region located between the binodal and spinodal line and the unstable region, located between the spinodal line and the polymer/CO_2 axis. The intersection of the binodal and spinodal curves occurs at the critical or plait point of the solution. Below

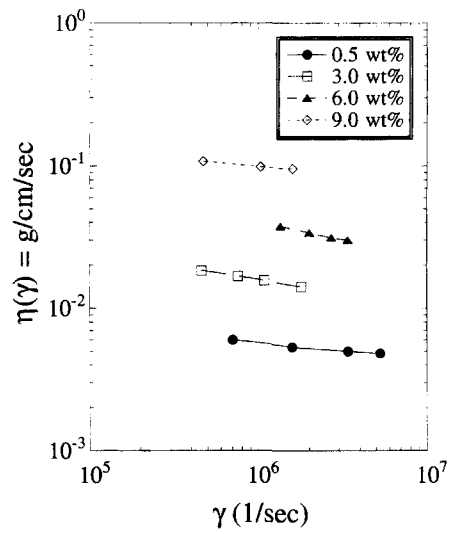

Figure 10 Non-Newtonian viscosity at the capillary wall as a function of shear rate and PC/SAN concentration (50/50 composition) in THF as determined by the Weissenberg–Rabinowitsch equation

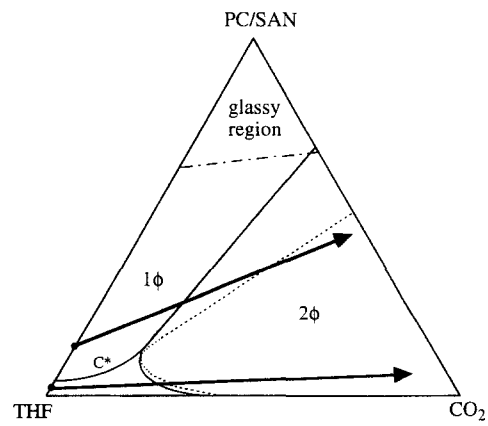

Figure 11 Ternary phase diagram showing mass transfer pathways for various PC/SAN in THF solutions precipitated into compressed CO_2. (—) Binodal line; (- - -) spinodal line; (- —) T_g line

the plait point concentration in the metastable region polymer discrete domains nucleate within a solvent continuous phase. Above the plait point concentration in the metastable region, solvent continuous domains nucleate within a polymer continuous fibre. The C^* concentration is near the plait point of the polymer solution[36]. The C^* concentration of the polymer solution increases with increasing antisolvent composition, since the reduction in solvent quality causes the chains to contract[26].

The C^* concentration for the PC–SAN/THF system may be estimated from scaling theory by $C^* \sim [\eta]^{1/2}$ where $[\eta]$ is the intrinsic viscosity[37]. The $[\eta]$ for pure PC and SAN in THF was obtained from the Mark–Houwink equation, $\eta = KM^a$, using K and a values obtained elsewhere[38]. For a good solvent and a theta solvent, the C^* concentrations are estimated to be 1.1 and 5.8 wt%, respectively, for PC and 1.4 and 13.2 wt% for SAN. For a 50/50 PC/SAN solution in THF/CO_2, the above values were averaged to estimate a C^* concentration between 1.0 to 10.0 wt%, respectively, along the mass transfer trajectory from a good to theta solvent in *Figure 11*.

The transition concentration for a change in morphology from particles to fibres for both PS in toluene and PAN in DMF was observed by Luna-Bárcenas *et al.*[26] to occur at approximately $3C^*$ (based upon a good solvent). As shown in *Figure 9(A,B)*, the PC/SAN morphology shifts from 0.1 to 0.5 μm primary microparticles to >10 μm particles as the solution concentration is increased from the dilute to semidilute regime, i.e. 0.5 to 3.0 wt%, respectively. Also, as mentioned above, the onset of chain entanglement at 3.0 wt% was confirmed visually during the sprays. The ~200% increase in viscosity supports this concept. Although the viscosity of the 3.0 wt% PC/SAN solution is observed to be too low to produce fibres, it is sufficient to dampen atomization. It is interesting that all three systems, PS, PAN and PC/SAN undergo the transition from particles to fibre formation at $\sim 3C^*$ (good solvent).

The last step in the discussion of the blend formation mechanism is to compare the times for polymer–solvent phase separation and for separation of the blend into two polymer phases. We begin by estimating the fastest possible times in both processes. For a homogeneous solution, the time for polymer–polymer phase separation is given by $\tau_{diff} = L^2/D_i$ where L is the process length scale and D_i is the polymer–polymer diffusivity[3]. The rate of polymer–polymer phase separation in a dilute solution is obtained by assuming a process length scale equal to the radius of gyration for a 10^5 molecular weight polymer, i.e. 10 nm, and a polymer diffusivity of 10^{-7} cm^2 s^{-1} [39]. Based upon these values, the minimum time for polymer phase separation in a dilute solution is 10^{-5} s.

The minimum characteristic times for polymer–solvent phase separation for a compressed fluid antisolvent and a conventional organic antisolvent are shown in *Table 3*. The maximum CO_2 diffusivity into the organic solution is 10^{-3} cm^2 s^{-1}, whereas, for an organic antisolvent, the diffusivity is only 10^{-5} cm^2 s^{-1} [40]. During jet breakup by atomization, the actual droplet sizes in the sprays are unknown. However, if 1.0 μm droplets were produced by capillary atomization, the minimum PCA quench time would be $\sim 10^{-5}$ s. On the other hand, if a fibre with a 100 μm o.d. were precipitated then the minimum quench time would be $\sim 10^{-1}$ s.

The actual characteristic times for polymer–solvent phase separation will be longer than above, as the diffusion coefficient of CO_2 in the polymer phase decreases as it dries. *Table 4* lists representative values of CO_2–solvent, CO_2–polymer, polymer–solvent and polymer–polymer binary diffusion coefficients, D, for various conditions. For example, D for CO_2 in PS is several orders of magnitude slower than in the initial droplets which are primarily organic solvent. Similarly, the polymer–polymer phase separation will slow down. For example, D for PS will decrease from 10^{-7} cm^2 s^{-1} in dilute solution to 10^{-9} cm^2 s^{-1} in 9.0 wt% solution and to 10^{-13} cm^2 s^{-1} in high M_W PS[41,42]. Because of the changing diffusion rates along the mass transfer pathway, the characteristic time for the PCA process cannot be determined from the degree of phase separation in the blend. This phase separation mechanism is further complicated by the different precipitation rates of the two polymers from THF.

Based upon the characteristic phase separation times and diffusion coefficients, we examine the results in *Figure 8*. For the 0.5 wt% PC/SAN solution ($C < C^*$), it is likely the atomization led to droplets on the order of 1.0 μm. This corresponds to a minimum PCA quench time of 10^{-5} s which is comparable to the minimum time for blend phase separation. The observation of single phase particles is consistent with this analysis, yet both times will become longer as the solution dries and becomes more viscous. As it dries, notice that D for CO_2 decreases from 10^{-3} to 10^{-6} cm^2 s^{-1} whereas D for the polymer decreases from 10^{-7} to 10^{-13} cm^2 s^{-1}.

Table 3 Comparison of minimum PCA quench time to that of a conventional organic antisolvent technique and RESS

Quench process	Characteristic quench time	Process length scale L_Q (μm)	D_i (cm^2 s^{-1}) or v_{SCF} (m s^{-1})	Minimum quench time (s)
Compressed fluid antisolvent (PCA)	$\tau_{PCA} = \frac{L_Q^2}{D_{CO_2}}$	1.0	10^{-3}	10^{-5}
		100	10^{-3}	10^{-1}
Organic antisolvent	$\tau_{org} = \frac{L_Q^2}{D_{org}}$	1.0	10^{-5}	10^{-3}
		100	10^{-5}	10^{1}
		1000	10^{-5}	$>10^{1}$
RESS	$\tau_{RESS} = \frac{L_Q}{v_{SCF}}$	30[a]	80–160[d]	10^{-6}–10^{-7}
		760[b]	10–80[d]	10^{-5}
		760[c]	0.5	10^{-3}

[a] Phase separation in nozzle
[b] Phase separation in nozzle entry
[c] Phase separation in preheater
[d] Axial distance vs velocity by Lele *et al.*[7]

Consequently, the time for polymer–polymer phase separation increases more than that for polymer–solvent phase separation. Thus, if PCA will trap a single phase blend based on the initial diffusion coefficients, the blend will not phase separate along the mass transfer pathway. These arguments also apply to the 3.0 wt% PC/SAN in THF/CO_2 solution where $C \sim C^*$.

For a 9.0 wt% PC/SAN in THF solution ($C > C^*$), a 100 μm fibre is formed. *Table 3* gives a minimum quench time for PCA of 10^{-1} s for a process length scale of 100 μm. Now the time for polymer–solvent phase separation exceeds that for polymer–polymer phase separation. Thus, the polymer blend has time to phase separate as observed. The formation of a dense skin on the fibre in the jet will further slow down the ability of CO_2 to quench the blend[35].

To highlight the rapid rate of polymer–solvent phase separation by PCA, estimates for the RESS process are also shown in *Table 3*. The characteristic quench time is given by $\tau_{RESS} = L_Q/\nu_{SCF}$ where the process length scale is the characteristic expansion dimension and ν_{SCF} is the velocity of the expanding supercritical fluid solution[3]. During expansion, polymer–solvent phase separation may occur within the nozzle, at the nozzle entrance or in the preheater[7–9]. The fluid velocity at each of these phase separation locations has been modelled by Lele and Shine[7]. When polymer–solvent phase separation occurs within the nozzle, the RESS quench time is between 10^{-6} and 10^{-7} s due to the rapid velocity (80–160 m s^{-1}) of the expanding solution. PEMA/PMMA blends were formed during this expansion condition. At the nozzle entrance, the solution velocity decreases to between 10 and 80 m s^{-1}, while the quench time increases to 10^{-5} s. Here the assumption was made that phase separation occurs in the preheater tubing (760 μm i.d.) leading up to the nozzle assembly. Phase separation in the preheater increases the quench time from 10^{-3} to 10^{-1} s. Because the RESS quench time was slower than the rate of polymer–polymer phase separation from a dilute solution (10^{-5} s), partially phase separated PEMA/PMMA blends composed of fibres and particles were produced when phase separation occurred in the preheater region of the expansion nozzle[7].

Table 3 shows that if phase separation occurs within a 30 μm orifice the quench time for RESS is 10^{-6}–10^{-7} s. On the other hand, the minimum time to quench a 1.0 μm droplet by PCA is one to two orders of magnitude slower at 10^{-5} s. However, both techniques have been shown to produce <1.0 μm microparticles and microspheres[9,14]. Theoretical models[7,43] and experimental results[43] have confirmed that a significant pressure drop occurs along the converging streamlines upstream of the expansion orifice in RESS. A pressure drop can supersaturate the supercritical fluid solution and increase the quench time significantly. This may explain why the minimum particle domain size is similar in RESS and PCA.

Effect of organic antisolvent

Our final objective is to compare the quench time of PCA to a conventional organic antisolvent technique. *Figure 12* shows the d.s.c. thermal curves obtained when a 3.0 wt% PC/SAN solution was either dripped into heptane from the 100 ml burette (1 mm droplets) or atomized from a 50 μm i.d. capillary nozzle (≈1 μm droplets) into heptane. The PC/SAN sample formed from the burette is shown to exhibit T_g behaviour similar to the curves observed for the 9.0 wt% PCA blend shown in *Figure 8*. Two T_g transitions occurring at 110 and 150°C are observed. When the precipitate was atomized into heptane, a single-T_g metastable blend is produced.

The organic antisolvent quench times calculated for the different process path lengths are shown in *Table 3*. The droplets emanating from the tip of the burette were observed to be approximately 10^3 μm in size. With this process length scale, the organic antisolvent quench time is well above 10^1 s. The slow quench time allows the solute to phase separate into primarily PC and SAN domains prior to vitrification. Similar behaviour was observed previously as a phase separated blend was also produced when a dilute PEMA/PMMA in chloroform solution was poured into methanol[3].

Although heptane is also able to produce a metastable blend for a 3.0 wt% PC/SAN solution, CO_2 offers advantages. Often the antisolvent to solvent ratio is 10:1 or even more. By replacing heptane with CO_2, the total organic solvent required for PC/SAN precipitation is reduced by 90%. The small amounts of solvent required for the polymer solution are easily removed from the precipitator by the continuously flowing CO_2, which dries the polymer. After 5 h drying of poly(L-lactic acid) micro-

Table 4 Summary of binary diffusion coefficient behaviour

System	T (°C)	Conditions	D (cm^2 s^{-1})	Ref.
CO_2–organic	60	80 bar	10^{-3}	39
	20	80 bar	10^{-4}	
CO_2–PS	25	>5 g CO_2/100 g PS	10^{-6}	28
	25	<5 g CO_2/100 g PS	10^{-7}	
CCl_4–PS	28	0.7 wt% ($C < C^*$)	10^{-7}	40
	28	4.0 wt% ($C > C^*$)	10^{-8}	
	28	9.0 wt% ($C > C^*$)	10^{-9}	
Labelled PS in PS	177	M_W = 18 000	$<10^{-11}$	41
	177	M_W = 161 200	$>10^{-13}$	

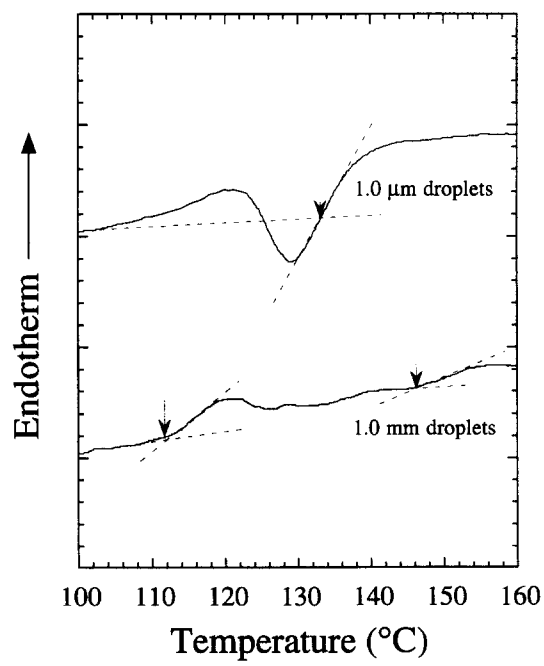

Figure 12 D.s.c. thermal curves of PC/SAN blends formed by precipitating a 3.0 wt% PC/SAN in THF solution at 1.0 ml min^{-1} into heptane at 23°C and 107 bar

spheres with supercritical CO_2, <100 ppm of residue methylene chloride was detected[44]. Conventional antisolvent precipitates require several days of vacuum drying at an elevated temperature. Aside from energy costs, vacuum drying can anneal the particles causing them to densify and become brittle.

Another advantage of PCA is that CO_2 would not be expected to form strong interactions with the organic antisolvent and the constituent homopolymers. Specific interactions between CO_2 and several Lewis bases have been observed recently with *FT*i.r. spectroscopy, although these interactions were weak when compared to many other specific interactions[31]. Strong specific interactions with the antisolvent are undesirable as they compete with interactions between the polymers and favour phase separation of the components of a blend. For example, PC and PMMA solutions in THF have been quenched by heptane into a metastable blend. However, a multiphase precipitate was formed when methanol was used as an antisolvent. Specific interactions form between the hydroxyl group of methanol and the carbonyl group of PC and PMMA[19].

CONCLUSIONS

Metastable PC/SAN polymer blends are formed by precipitation with a compressed fluid antisolvent, specifically liquid carbon dioxide. In supercritical CO_2 at 35°C, the blends phase separate due to plasticization of SAN by CO_2. At temperatures below 25°C, a metastable blend is formed for polymer concentrations up to 3.0 wt%, as the minimum quench time for PCA is on the order of the minimum time for polymer–polymer phase separation. As the solution dries along the mass transfer pathway, the time for polymer–polymer phase separation will increase by more than the PCA quench time. Thus if a single phase blend is trapped based upon a comparison of minimum times for phase separation, then the blend will remain as a single phase over the entire mass transfer pathway. At higher concentrations above $3C^*$ (good solvent) where significant chain entanglement occurs, i.e. 9.0 wt% PC/SAN, 100 μm fibres are formed. The minimum quench time increases to 0.1 s which allows the polymer chains to phase separate. For a conventional liquid antisolvent, the quench time is two orders of magnitude higher due to the slower diffusivity of the organic antisolvent.

ACKNOWLEDGEMENTS

Financial support of the work was provided by the National Science Foundation Grant No. CTS-9218769, the Texas Advanced Technology Program Grant No. 3658-198 and the Separation Research Program at the University of Texas. We thank Prof. Donald R. Paul at UT and Prof. Annette D. Shine at the University of Delaware for many helpful discussions.

REFERENCES

1. Cutright, D. E., Perez, B., Beasley, J. D., Larson, W. J. and Posey, W. R., *Oral Surg.*, 1974, **37,** 142.
2. Nauman, E. B., Ariyapadi, M. V., Alsara, N. P., Grocela, T. A., Furno, J. S., Liu, S. H. and Mallikarjun, R., *Chem. Eng. Commun.*, 1988, **66,** 29.
3. Boen, S. N., Bruch, M. D., Lele, A. K. and Shine, A. D., in *Polymer Solutions, Blends and Interfaces*, ed. I. Noda and D. N. Rubingh. Elsevier, Amsterdam, 1992, pp. 151–172.
4. Matson, D. W., Fulton, J. L., Peterson, R. C. and Smith, R. D., *Ind. Eng. Chem. Res.*, 1987, **26,** 2298.
5. Peterson, R. C., Matson, D. W. and Smith, R. D., *Polym. Eng. Sci.*, 1987, **27,** 1693.
6. Lele, A. K. and Shine, A. D., *AICHE J.*, 1992, **38,** 742.
7. Lele, A. K. and Shine, A. D., *Ind. Eng. Chem. Res.*, 1994, **33,** 1476.
8. Tom, J. W., Debenedetti, P. G. and Jerome, R., *J. Supercrit. Fluids*, 1994, **7,** 9.
9. Mawson, S. M., Johnston, K. P., Combes, J. R. and DeSimone, J. M., *Macromolecules*, 1995, **28,** 3182.
10. DeSimone, J. M., Guan, Z. and Elsbernd, C. S., *Science*, 1992, **257,** 945.
11. Hsiao, Y. L., Maury, E. E., DeSimone, J. M., Mawson, S. M. and Johnston, K. P., *Macromolecules*, 1995, **28,** 8159.
12. Tom, J. W. and Debenedetti, P. G., *J. Aerosol Sci.*, 1991, **22,** 555.
13. Tom, J. W. and Debenedetti, P. G., *Polym. Prepr.*, 1992, **33,** 104.
14. Dixon, D. J., Bodmeier, R. A. and Johnston, K. P., *AIChE J.*, 1993, **39,** 127.
15. Yeo, S., Lim, G., Debenedetti, P. G. and Bernstein, H., *Biotech. Bioeng.*, 1993, **41,** 341.
16. Randolph, T. W., Randolph, A. D., Mebes, M. and Yeung, S., *Biotechnol. Progr.*, 1993, **9,** 429.
17. Dixon, D. J., ed., *Formation of Polymer Materials by Precipitation with a Compressed Fluid Antisolvent*. The University of Texas at Austin, 1992.
18. Bodmeier, R., Wang, H., Dixon, D. J., Mawson, S. and Johnston, K. P., *Pharmac. Res.*, 1994, **12,** 1211.
19. Chiou, J. S., Barlow, J. W. and Paul, D. R., *J. Polym. Sci.: Part B: Polym. Phys.*, 1987, **25,** 1459.
20. Wissinger, R. G. and Paulaitis, M. E., *J. Polym. Sci., Part B, Polym. Phys.*, 1991, **29,** 631.
21. Condo, P. D. and Johnston, K. P., *J. Polym. Sci.: Part B, Polym. Phys.*, 1992, **32,** 523.
22. Condo, P. D., Paul, D. R. and Johnston, K. P., *Macromolecules*, 1994, **27,** 365.
23. Handa, Y. P., Lampron, S. and O'Neill, M. L., *J. Polym. Sci: Part B: Polym. Phys.*, 1994, **32,** 2549.
24. Wisniewski, C., Marin, G. and Monge, P., *Eur. Polym. J.*, 1985, **21,** 479.
25. Callaghan, T. A., Takakuwa, K., Paul, D. R. and Padwa, A. R., *Polymer*, 1993, **34,** 3796.
26. Luna-Bàrcenas, G., Kanakia, S. K., Sanchez, I. C. and Johnston, K. P., *Polymer*, 1995, **74,** 1.
27. Beckman, E. and Porter, R. S., *J. Polym. Sci.*, 1987, **25,** 1511.
28. Berens, A. R. and Huvard, G. S., in *Supercritical Fluid Science and Technology*, Vol. 406, ed. K. P. Johnston and J. M. L. Penninger. ACS, Washington, DC, 1989, pp. 207–223.
29. Bosma, M., Brinke, G. and Ellis, T. S., *Macromolecules*, 1988, **21,** 1465.
30. Pochan, J. M., Beatty, C. L. and Pochan, D. F., *Polymer*, 1979, **20,** 879.
31. Meredith, J. C., Johnston, K. P., Seminario, J. M. Kazarian, S. G. and Eckert, C. A., *J. Phys. Chem.*, 1995, **100,** 10837.
32. Chiou, J. S., Barlow, J. W. and Paul, D. R., *J. Appl. Polym. Sci.*, 1985, **30,** 2633.
33. Lefebvre, A. H., *Atomization and Sprays.*, Hemisphere, New York, 1989.
34. Bayvel, L. and Orzechowski, Z., *Liquid Atomization.*, Taylor and Francis, Washington, DC, 1993.
35. Dixon, D. J. and Johnston, K. P., *J. Appl. Polym. Sci.*, 1993, **50,** 1929.
36. Sanchez, I. C. in *Encyclopedia of Physical Science and Technology*, Vol. 13. Academic Press, 1992, pp. 153–170.
37. Rinaudo, M., *J. Appl. Polym. Sci., Appl. Polym. Symp.*, 1993, **52,** 11.
38. Kurata, M. and Tsunashima, Y., *Polymer Handbook*, ed. J. Brandrup and E. H. Immergut. J. Wiley and Sons, New York, 1989.
39. Lechner, M. D. and Steinmeier, D. G., *Polymer Handbook*, ed. J. Brandrup and E. H. Immergut. J. Wiley and Sons, New York, 1989.
40. McHugh, M. A. and Krukonis, V. J., *Supercritical Fluid Extraction Principles and Practice*, 2nd edn. Butterworths, Stoneham, MA, 1994.
41. Callaghan, P. T. and Pinder, D. N., *Macromolecules*, 1981, **14,** 1334.

42. Ye, M., Composto, R. J. and Stein, R. S., *Macromolecules*, 1990, **23,** 4830.
43. Berends, E. M., Supercritical Crystallization: The RESS-Process and the GAS-Process, Ph.D. thesis, Delft Technical University, Delft, 1994.
44. Ruchatz, R. and Müller, B. W., *Influence of Production Conditions of the ASES Process on Microparticle Properties*. Austin, TX, 1995.